

University of South Dakota

USD RED

---

Honors Thesis

Theses, Dissertations, and Student Projects


---

Spring 5-8-2021

# Suzuki Coupling Catalyzed by (8-(dimesitylboryl)quinoline)palladium(0) Species: A Theoretical Analysis

Haley S. Rust  
*University of South Dakota*

Follow this and additional works at: <https://red.library.usd.edu/honors-thesis>

 Part of the [Inorganic Chemistry Commons](#), and the [Physical Chemistry Commons](#)

---

## Recommended Citation

Rust, Haley S., "Suzuki Coupling Catalyzed by (8-(dimesitylboryl)quinoline)palladium(0) Species: A Theoretical Analysis" (2021). *Honors Thesis*. 155.  
<https://red.library.usd.edu/honors-thesis/155>

This Honors Thesis is brought to you for free and open access by the Theses, Dissertations, and Student Projects at USD RED. It has been accepted for inclusion in Honors Thesis by an authorized administrator of USD RED. For more information, please contact [dloftus@usd.edu](mailto:dloftus@usd.edu).

## CHAPTER ONE

### Introduction

Lewis bases are known as being donors of electron pairs and the Lewis acids are known for being acceptors of these electron pairs. Frustrated Lewis pairs have a structure containing both a Lewis acid and a Lewis base unable to neutralize each other due to geometric constraints. Another term for this type of compound is LXZ ligands where L is a Lewis base and Z is a Lewis acid, while X can be identified as electron donor and acceptor ligands (e.g., transition metals). Electrons are donated from the L ligand to the X center, that then donates electrons to the Z ligand. **Figure 1** depicts the type of interaction these ligands will have in a reaction involving fluorine on the opposing compound.

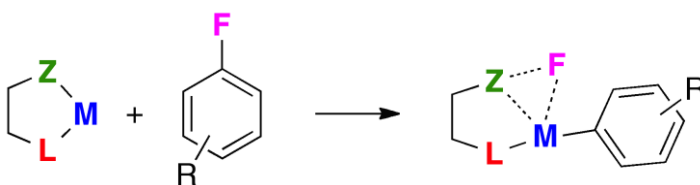


**Figure 1.** The relationship between the Metal, Z-ligand, L-ligand, and fluorine (F) involved in our desired synthesis reaction.

The F interaction that was mentioned is important to break a C-F bond resulting in a novel complex. This is a very difficult and thermodynamically unfavorable reaction in many cases due to the high bond enthalpy of the C-F bond and being a non-polarizable bond.

This work was inspired by Harman and Peters[1] work with a H<sub>2</sub> molecule and oxidative addition where they attracted a hydrogen (H) molecule leading to bridging the M and Z centers (Ni and boron (B) respectively).

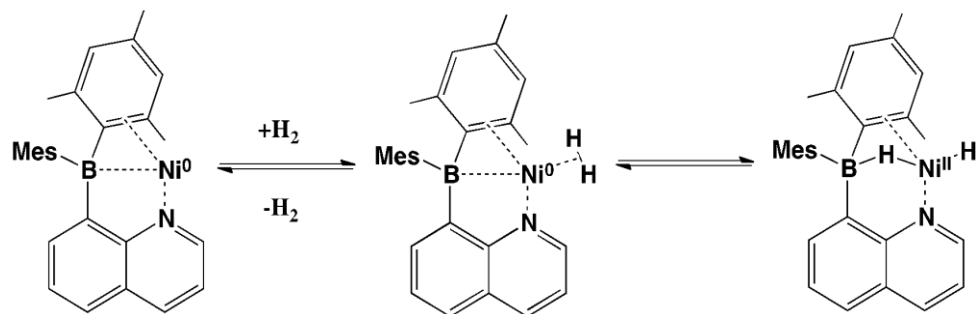


**Figure 2.** The reversible activation of H<sub>2</sub> and the formation of bridging H between the Ni and B centers.

The frustrated Lewis pair species is the (quinolin-8-yl)dimesitylborane (DMBQ) ligand (**Figure 3**). The top half of the compound, two mesityls and the B center, produce the Lewis acid (Z ligand). The bottom half is a quinoline ring that provides the ligand structure with the Lewis base (L ligand). This ligand can coordinate a transition metal at the L site that could donate electrons to the boron center. An investigation of d<sup>10</sup> transition metals (Ni, Pd, and Pt) to determine which thermodynamically favors the cleavage of C-F bonds as well as catalyze other relevant reactions such as the C-C bond formation via the Suzuki cross-coupling reaction.

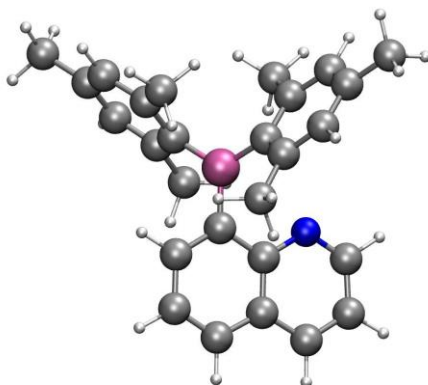


**Figure 3.** An illustration of the (quinolin-8-yl)dimesitylborane (DMBQ) ligand.

To activate a C-F bond, the  $d^{10}$  transition metal undergoes oxidative addition.[2] This oxidative addition reaction has been proven to work in the case of  $H_2$  bonds.[1] After the cleavage of the C-F bond, the F will bond with the transition metal in the complex possibly bridging between the B and the metal, while the C will bond with the transition metal.

**Figure 4** below illustrates an LMZ ligand that could result from the synthesis involving group X transition metals reacting with  $CH_3F$ . Instead of DMBQ, this compound has chlorine (Cl) bonded to one of the mesityl groups involved in the Z ligand (DMBQ-Cl). With the help of theoretical calculations, the thermodynamics of the DMBQ-Cl complex reacting with  $CH_4$  and  $CH_3F$  and breaking the carbon-hydrogen (C-H) bond and C-F bond, respectively, could be predicted. Referring to **Table 1**, the C-F bonds have activation energies with all three  $d^{10}$  transition metals that are much more favorable than the C-H bonds. From this data, the conclusion was made that interacting the metal complex with a C-F molecule is much more desirable than a molecule containing C-H bonds.

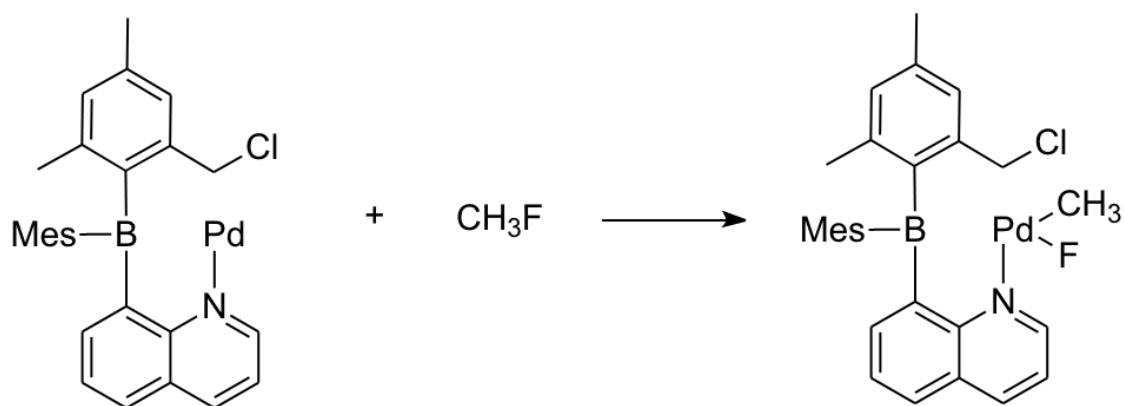


**Figure 4.** The reaction of  $\text{CH}_3\text{F}$  with a DMBQ-Cl coordinated to the palladium center and the breaking the C-F bond.

**Table 1:** Gibbs free energy for the C-H and C-F cleavage in  $\text{CH}_4$  and  $\text{CH}_3\text{F}$  by DMBQ-Cl-X(0).

Transition Metal (X)	$\text{CH}_3\text{F}$ Bonds $\Delta G$ (kcal/mol)	$\text{CH}_4$ Bonds $\Delta G$ (kcal/mol)
<b>Pd</b>	-2.9	62.8
<b>Pt</b>	-15.3	48.3
<b>Ni</b>	-12.7	27.7

In **Figure 5**, the overall reaction process that is intended is illustrated. First, DMBQ is synthesized. Next, determine which  $d^{10}$  transition metal (Ni, Pd, Pt) is best according to theoretical calculations and undergo metalation with DMBQ forming DMBQ-X(0). Lastly, complete oxidative addition of a C-F bond to result in the novel complex with a newly reduced transition metal, X(II).

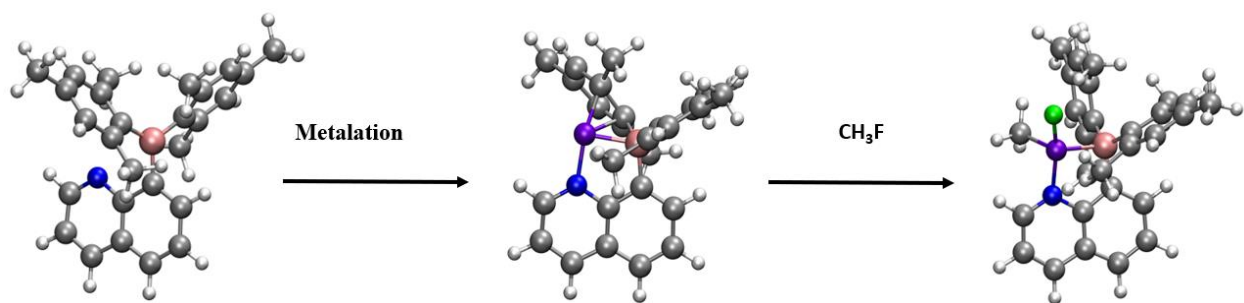


**Figure 5.** Metalation and oxidative addition of the CH<sub>3</sub>F C-F bond. Color code: F in green, B in pink, and transition metal in purple.

## CHAPTER TWO

### Computational Details

All geometries were fully optimized using density functional theory (DFT) implementation in the Gaussian 16 package.[3] The M06-L exchange-correlation functional was used in conjunction with the def2-TZVP basis set on all atoms.[4-6] The nature of all stationary points and transition states was verified by analytic computation of vibrational frequencies. These were employed for the computation of zero-point vibrational energies and the molecular partition functions for use in computing standard state free energy energies. The solvent effects of methanol and tetrahydrofuran (THF) were included with the solvation model based on density (SMD).[7] Bond orders and the topological analysis of the electron density was performed using Multiwfn 3.5.[8] ETS-NOCV calculations were performed using Amsterdam Density Functional (ADF).[9-10]

## CHAPTER THREE

### Results

Experimentally, the inorganic synthesis of the frustrated Lewis pair, DMBQ, began. This compound must be synthesized prior to metalation with a  $d^{10}$  transition metal and, ultimately, oxidative addition with a C-F bond. The first step is reacting 8-aminoquinoline with sodium nitrate ( $\text{NaNO}_2$ ) with potassium iodide (KI) at a temperature between 0-5 degrees Celsius. The mixture sat overnight but the 8-iodoquinoline was not successfully synthesized the first time the synthesis was attempted. This raised questions as to how thermodynamically favorable this reaction was (**Figure 6**).

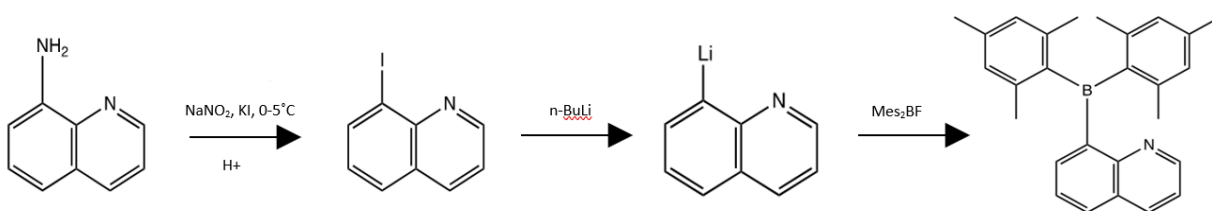


**Figure 6.** Reaction scheme for the experimental synthesis of the Frustrated Lewis Pair, DMBQ.

Computational researchers began to determine which halogen variation (iodine (I), bromine (Br), Cl) of the first product, 8-Xquinoline, would result in the most thermodynamically favorable pathway to acquire 8-lithiumquinoline. This is the second reaction in the experimental scheme and is the lithiation step due to reacting with butyl lithium (n-BuLi). Below are the reaction schemes illustrating 8-iodoquinoline (**Figure 7**),



8-bromoquinoline (**Figure 8**), and 8-chloroquinoline (**Figure 9**) as the second product in the experimental scheme undergoing lithiation giving us 8-lithiumquinoline.



**Figure 7.** 8-iodoquinoline reacting with n-BuLi to result in 8-lithiumquinoline and n-BuI products.

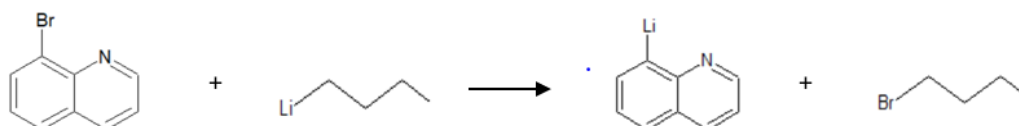


**Figure 8.** 8-bromoquinoline reacting with n-BuLi to result in 8-lithiumquinoline and n-BuBr products.



**Figure 9.** 8-chloroquinoline reacting with n-BuLi to result in 8-lithiumquinoline and n-BuCl products.

Computationally, the next goal was to determine which halogen would act as the best leaving group and give the most thermodynamically favorable pathway. Referring to **Table 2**, the Gibbs free energies for each of these reactions listed in kcal/mol values. Br appears to be the most favorable halogen. Cl and I are very similar in Gibbs free energy values and

not far from Br. This gave experimental researchers confidence to continue with 8-iodoquinoline and retry the synthesis despite the difficulty.

**Table 2.** Gibbs free energy values (kcal/mol) of halogen X replacement by lithium (X=I, Br, or Cl).

Halogen (X)	$\Delta G$ (kcal/mol)
I	-22.72
Br	-23.41
Cl	-22.77

Experimentally, synthesis of 8-iodoquinoline was restarted. 8-aminoquinoline reacted with the same reagents,  $\text{NaNO}_2$  and KI, but the reaction beaker was submerged in a liquid nitrogen bath. This kept the reaction well below 0 degrees Celsius, which was a different environment compared to the first attempt at synthesis. Experimentalists added stirring rods to keep the mixture from solidifying. The mixture was then allowed to warm to room temperature for an hour, then the decision to heat up the reaction was made. The pH of the mixture was very acidic. Sodium hydroxide (NaOH) and potassium hydroxide (KOH) were added to the solution to raise pH and return to a basic range. Toluene was added to the mixture and was intended to extract our 8-iodoquinoline. The rotary evaporator was used to separate toluene, which had a pink hue from our 8-iodoquinoline. The color change in the toluene signified that iodine may have been extracted during the rotary evaporator step. Next, sodium thiosulfate solution was added to mixture to remove any iodine impurities that may be interfering with the desired product. This mixture was placed in a separation funnel where 8-iodoquinoline would be isolated from any impurities in the mixture. Since

8-iodoquinoline has a lower density than other immiscible liquids in the mixture, it will be found in the top layer and allow for proper extraction.

A proton Nuclear Magnetic Resonance (NMR) spectrum was very important at this stage to ensure the product contained 8-iodoquinoline. The solvent used was deuterated chloroform due to this solvent not having any excess protons that would interfere with the NMR reading. The experimental NMR is shown below in **Figure 10**. The expectation was to have six identifiable peaks in NMR due to 8-iodoquinoline. The spectra confirmed that 8-iodoquinoline was in solution.

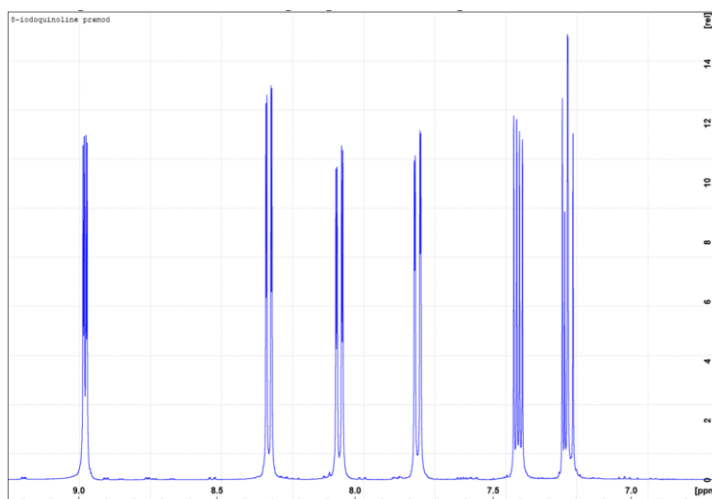


**Figure 10.** Experimental proton NMR of 8-iodoquinoline using deuterated chloroform as solvent.

A model proton NMR of 8-iodoquinoline was created computationally as well. This insight to where the peaks came from, which proton was signified by which peak on the NMR. It also reassured experimentalists in the product created from the first step of synthesis. Theoretical calculations gave 8-iodoquinoline proton values in parts per million (ppm). An

experimental NMR shifts these values using tetramethylsilane (TMS), which has a value of 31.871 ppm. TMS is the starting point of an NMR, it is signified by the 0 on the x-axis. The equation used to calculate these values theoretically is  $\delta = \sigma_{\text{ref}} - \sigma$ . The theoretical proton value was subtracted from the TMS value to result in the shifted proton values in ppm. The results of these calculations can be found in **Table 3**. **Figure 11** shows 8-iodoquinoline with color coded dots over the protons that coincide with the colors in **Table 3** to illustrate which proton resulted in which value.

**Table 3.** Theoretical proton values of 8-iodoquinoline in ppm. The shifted values in ppm after using the equation and TMS as reference point.

Color Code	8-Iodoquinoline (ppm)	Shifted Value (ppm)
Hydrogen 1	23.581	8.170
Hydrogen 2	24.287	7.464
Hydrogen 3	24.010	7.741
Hydrogen 4	23.596	8.154
Hydrogen 5	22.795	8.956
Hydrogen 6	24.363	7.388

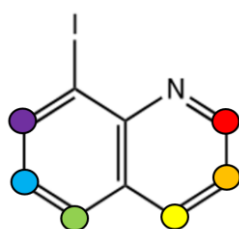


**Figure 11.** 8-iodoquinoline with color coding to signify which proton on the structure relates to which theoretically calculated values in ppm.

Since identification of 8-iodoquinoline has been done both experimentally and computationally, it was time to continue onto the second reaction in experimental synthesis. Referring back to **Figure 6**, the next step is to perform the lithiation step using n-BuLi. The 8-iodoquinoline was first dissolved in tetrahydrofuran (THF), then n-BuLi was added using a canula transfer. The final step of the reaction synthesis was completed simultaneously by adding dimesityl boron fluoride ( $\text{Mes}_2\text{BF}$ ) via canula transfer. The mixture was left to sit overnight. The color of precipitant was a very dark black-brown color. Experimentalists began the process of working up the mixture by vacuuming off the THF. The residual product was a dark red gooey substance. Then, observations were made in hopes of crystals crashing out. When they did not appear, the decision was made to leave the mixture overnight once again. No crystals were found the next morning and the decision was made to add pentane. The solution was filtered but no precipitate was found. Toluene was added to the mixture and allowed to sit overnight. After once again not finding crystals, pentane was added to the supernatant. At this point, the conclusion was made that the first run reaction scheme was unsuccessful. The yield of DMBQ, if any, was so small that synthesis could not move forward with the metalation step. The synthesis of DMBQ would take much more time to perfect and complete. My efforts were then refocused to being entirely computational calculations to find thermodynamically favorable pathways to lay the roadmap for future experimental research.

The next computational objective was to find which reaction pathway was most likely to occur between the 8-lithiumquinoline and  $\text{Mes}_2\text{BF}$  to result in DMBQ and lithium fluoride (LiF). **Figure 12** illustrates two reaction pathways, a single-step and a two-step. The single-step reaction pathway has a Gibbs free energy value of -8.07 kcal/mol. The other reaction

pathway that consists of two steps is unlikely to occur. The first reaction has a Gibbs free energy of 101.9 kcal/mol, showing it is an unstable intermediate. Then it is followed by the second reaction with a Gibbs free energy value of -109.9 kcal/mol. The first reaction of the two-step pathway has an extreme Gibbs free energy value that is unlikely to be overcome. It is much more likely for the last step of our DMBQ reaction synthesis in **Figure 12** to be completed in by the one-step pathway versus the two-step.

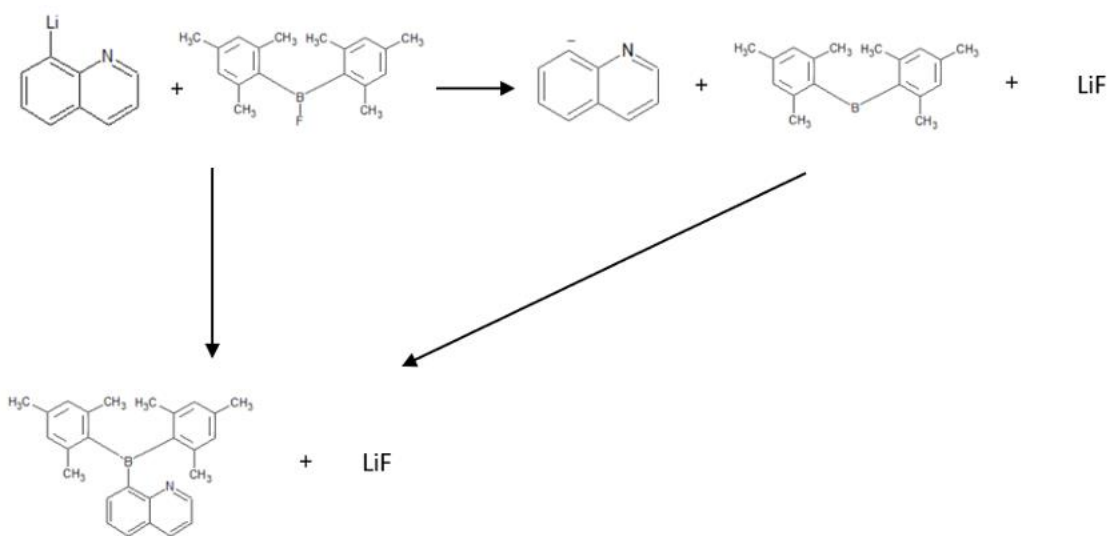


**Figure 12.** Potential reaction pathways for 8-lithiumquinoline and Mes<sub>2</sub>BF to get products DMBQ and LiF

The next step was to calculate the strength of the bonds between atoms using Laplacian bond order (LBO). The compound in question is DMBQ-Cl complexed with one of the d<sup>10</sup> transition metals (Ni, Pd, Pt), which will be referred to as DMBQ-Cl-M. This compound is shown in **Figure 13**. These calculations evaluate the strength of B-M, N-M and C-C-M interactions. The results of these calculations are listed in **Table 4**. None of the LBO values

that we found were significant enough to show the interactions that we were expecting to find between one of the metals and the rest of the atoms in the compound. There is actually no LBO value between the metals Pd or Pt with the B of the DMBQ-Cl-M structure. A significant LBO value would have indicated which  $d^{10}$  transition metal would be the best for the research circumstances. The distance between the metals and other atoms in optimized structures are shown in **Table 4** as well, they are the values in parenthesis and are in the unit of Angstroms.

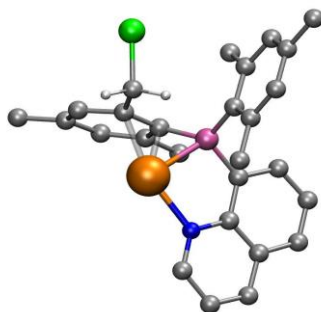


**Figure 13.** DFT optimized geometry of DMBQ-Cl-M species.

**Table 4:** LBOs for selected bonds and distances (in Angstroms) shown in parentheses.

	Ni	Pd	Pt
<b>B-M</b>	0.06 (2.103)	- (2.221)	- (2.194)
<b>N-M</b>	0.31 (1.911)	0.21 (2.165)	0.23 (2.113)
<b>C-C-M</b>	0.16 (1.958)	0.10 (2.164)	0.11 (2.133)

Dr. Hoefelmeyer had synthesized the desired frustrated Lewis pair, DMBQ, in the past.[11] They revealed the bond lengths of his synthesized DMBQ in their published article using the Bruker SMART Apex II Diffractometer with CCD area detector. With this information in mind, DMBQ was optimized computationally, and the bond lengths were found. **Figure 14** illustrates the crystallized DMBQ-Cl structure with Pd as the  $d^{10}$  transition metal.[11] **Table 5** shows the experimental and theoretical bond distances in Angstroms. Comparisons between DMBQ theoretically and experimentally were made. Any difference between the two compared values that is less than 0.1 Angstrom is considered acceptable. All of the bond length differences fell within that acceptable range. **Table 6** also shows the experimental and computational values of the C9-C8-B angle. The difference between the two was 0.1 degrees, which is also considered to be acceptable.

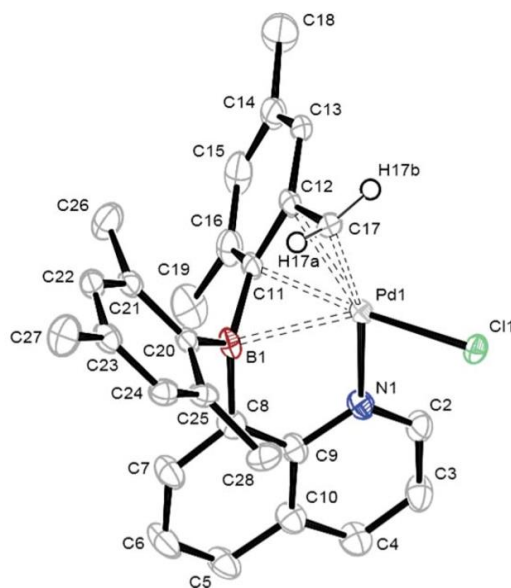


**Figure 14.** Crystallized DMBQ-Cl molecule complexed with palladium.[11]



**Table 5.** Comparisons of experimental[11] and computational bond lengths in Angstroms.

<b>Bond Name</b>	<b>Literature (Å)</b>	<b>M06L/def2-TZVP (Å)</b>
<b>Pd(1)-C(17)</b>	2.074	2.075
<b>Pd(1)-N(1)</b>	2.118	2.172
<b>Pd(1)-C(11)</b>	2.168	2.183
<b>Pd(1)-C(12)</b>	2.248	2.225
<b>Pd(1)-Cl(1)</b>	2.349	2.398
<b>Pd(1)-B(1)</b>	2.379	2.351

**Table 6.** Comparison of experimental[11] and computational C9-C8-B angle values in degrees.

<b>Angle Name</b>	<b>Literature (Degree)</b>	<b>M06L/def2-TZVP (Degree)</b>
<b>C(9)-C(8)-B(1)</b>	123.4	123.5

**Figure 15** illustrates a reaction found in that same publication by Dr. Hoefelmeyer.[11] and the Gibbs free energy values that were found theoretically in kcal/mol to determine the thermodynamic favorability of this reaction. DMBQ undergoes a hydrolysis reaction to result in the first transition state. The Gibbs free energy value of reaching this first transition state is +3.8 kcal/mol, which is kinetically favorable. The transition state lost a mesitylene group resulting in a decrease in Gibbs free energy with a value of -48.8 kcal/mol. This compound undergoes the second hydrolysis reaction of this scheme producing the second transition state. There is once again an increase in Gibbs free energy, +12.2 kcal/mol, which is kinetically favorable. The loss of a second methylene causes a decrease in Gibbs free energy from the second transition state with a value of -46.2 kcal/mol. For the final reaction of the scheme, a condensation reaction between two of the resulting species lead to the

formation of a dimeric structure with a Gibbs free energy value of +8.3 kcal/mol. **Figure 16** depicts the molecular orbitals of DMBQ-Cl-Ni found computationally. They are in agreement with a fully occupied d orbital in the Ni.

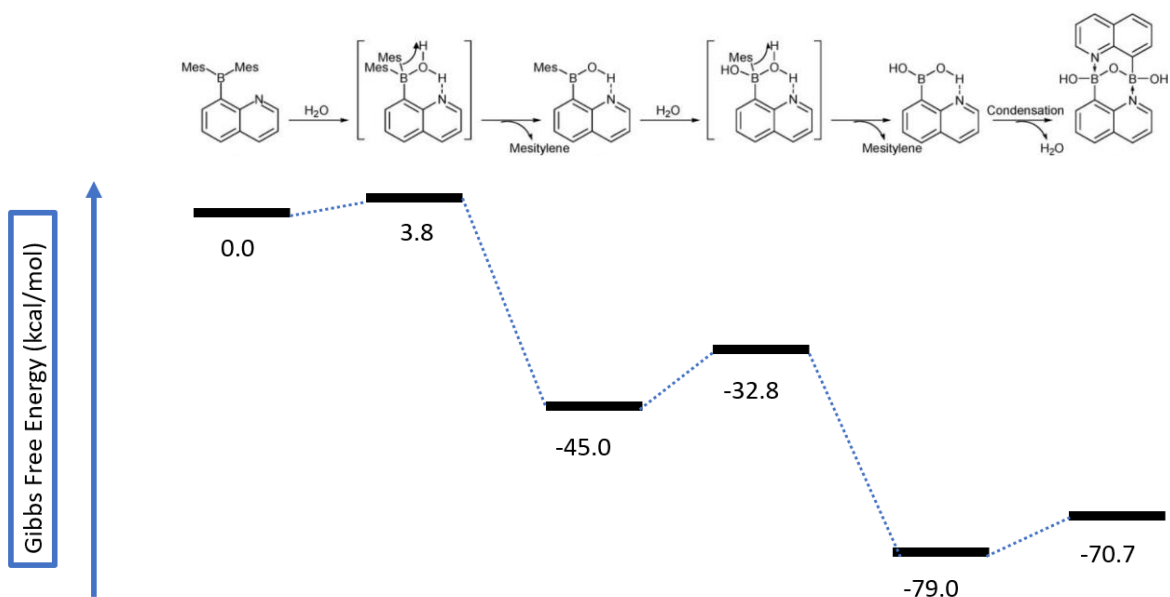


**Figure 15.** Reaction scheme of DMBQ and the associated Gibbs free energies (kcal/mol).

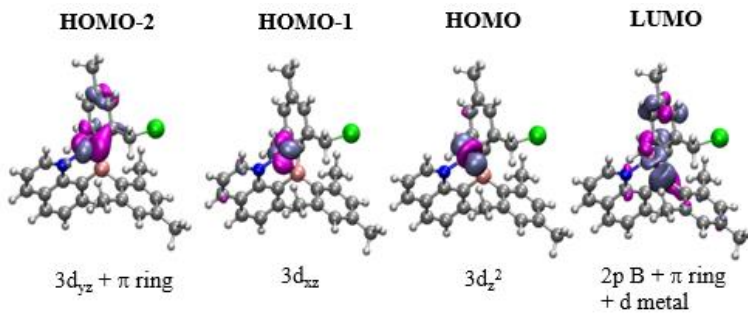


**Figure 16.** Frontier molecular orbitals of DMBQ-Cl-Ni and components.

For a majority of the research, we were under the impression that DMBQ-Cl was the compound that would undergo the metalation step, with Pd, and ultimately complete oxidative addition to break the C-F bond and create a novel complex. At this point, the realization was made that this was not the case. In **Figure 17**, we show DMBQ-Cl undergoing metalation with  $L_2PdCl_2$  as the reagent. This resulted in a compound that has Pd with an oxidation state of II. We need Pd to have an oxidation state of 0 in order to work properly as the catalyst for the Suzuki cross-coupling reaction mechanism.

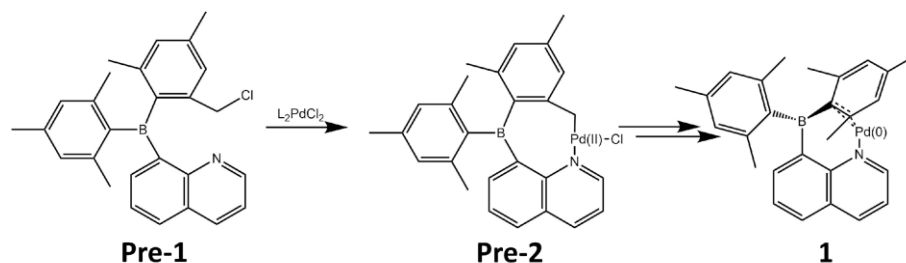


**Figure 17.** Illustrates the reaction scheme of DMBQ-Cl undergoing metalation and transforming into the desired catalyst.

The Gibbs free energy diagram for finding the Pd(0) catalyst that would ultimately be used in the Suzuki cross-coupling reaction mechanism can be found in **Figure 18**. The values shown are Gibbs free energy measurements in kcal/mol. The energy diagram begins with the DMBQ-Cl-Pd(II) complex (**Pre-2**). One of the proposed reactions to reach the desired catalyst was a reductive elimination reaction. This reaction is indicated by the blue line, it is very thermodynamically unfavorable (+32.6 kcal/mol) due to the difficulty of breaking the bond between Pd and methyl group. The reaction scheme indicated with the black line

is the pathway that is thermodynamically favorable in the pursuit of the catalyst. Many of the reactions and reagents involved in this pathway resemble a Suzuki cross-coupling reaction. For instance, the first reaction replaces the halogen (Pd-Cl) with a hydroxide (Pd-OH). This is referred to as a ligand exchange. The second reaction, Pd-OH to Pd-Ph, resembles a transmetallation reaction due to the substrate reacting with boronic acid. This results in the hydroxide being replaced by an R group, a phenyl in this case. The third reaction, compound Pd-Ph to compound Pd-Ph(OCH<sub>3</sub>), an R group (methoxy) is added to the Pd. For the fourth reaction, Pd-Ph(OCH<sub>3</sub>) to Pd-Ph<sub>2</sub>, another transmetallation reaction is observed due to an R group (phenyl) replacing the methoxy group. Lastly, Pd-Ph<sub>2</sub>, to **1** we observe a reductive elimination reaction and an intermediate transition state. Thus, producing the desired DMBQ-Pd(0) catalyst.

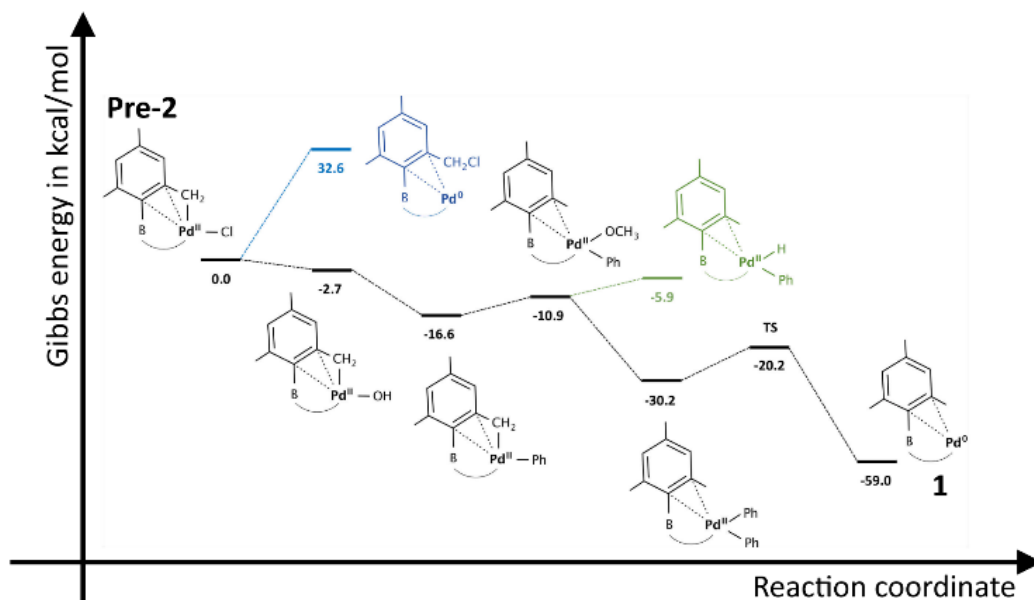


**Figure 18.** Gibbs free energy diagram for synthesizing our Suzuki cross-coupling catalyst, **1**. Values are shown in kcal/mol.

Now that the relationship between **Pre-2** and **1** has been recognized, it is important to explore the interactions between the atoms in these two compounds. **Figure 19** shows the first derivative of the electron densities between atoms. The scale to the right of the diagram shows the connection between color and number value. The dark blue, value 0, shows maximums or minimums. It also signifies that there is a sigma bond found in that space. The main interaction in question is between the B and Pd, 0 and II, atoms. The left image of **Figure 19** shows compound **Pre-2** and the right image shows compound **1**. There is not a maximum/minimum value observed between the B and Pd(II) in compound **Pre-2** or between B and Pd(0) in compound **1**.

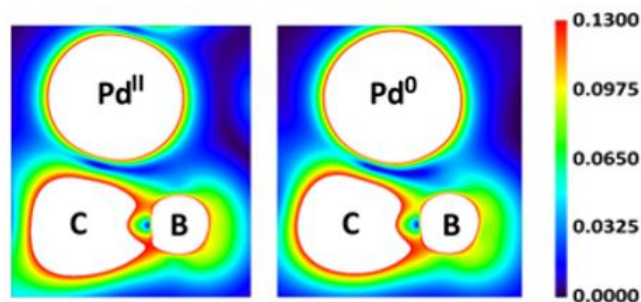


**Figure 19.** **Pre-2** (left) and **1** (right) first derivative of electron densities.

**Figure 20** shows the second derivative of the electron densities, also referred to as Laplacian. Once again, compound **Pre-2** is the left image and **1** is the right image. For the second derivative of the electron densities, we are looking for a negative value that is indicated by a dark blue, or black, color. The desired relationship is observed between the C and B of both compounds, which is an interaction we are fully aware of. Unfortunately, no interaction, or sigma bond, is observed between B and Pd(II) or Pd(0).

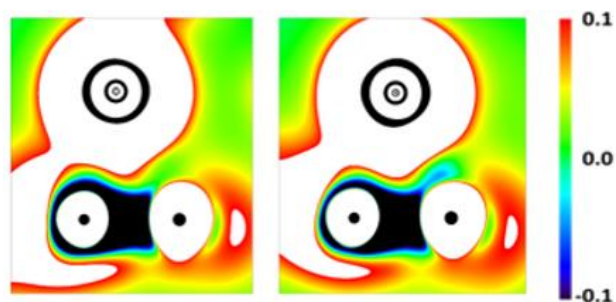


**Figure 20.** **Pre-2** (left) and **1** (right) second derivative of electrons densities.

In the two figures below, **Figure 21** and **Figure 22**, ETS-NOCV calculations were performed to illustrate the deformation density of the orbitals. ETS being an abbreviation for the extended transition state method. NOCV is an abbreviation for natural orbitals for chemical valence theory. This calculation tool has also been referred to as EDA-NOCV, energy decomposition analysis (EDA). The interactions between the atoms in compound **1** and **Pre-2** are once again being observed. In **Figure 21**, showing compound **Pre-2**, the electron density is largely focused on the Cl of the structure. The Cl atom is attracting electrons away from the electron deficient B, which explains why compound **Pre-2** is high in energy and unfavorable compared to our catalyst, compound **1**. Considering compound **1**, the deformation density of the orbitals illustrates that electrons are being donated to the B of the complex (**Figure 22**). The electrons are coming from the nitrogen, through the Pd and to the B atom. This is the exact type of atomic-level relationship needed to prove our compound **1** is a proper LMZ ligand. These electrons are transformed through this interaction and result in a thermodynamically favorable compound, the catalyst for the Suzuki cross-coupling reaction mechanism.

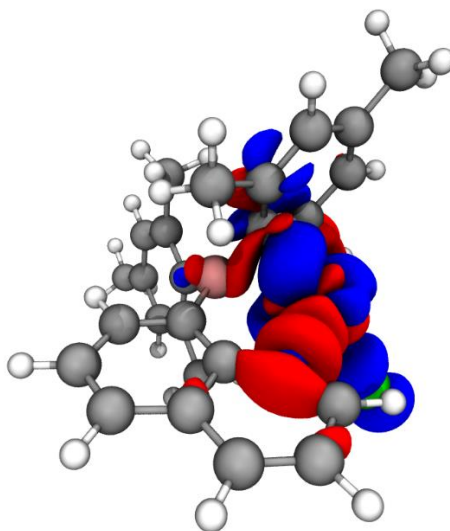


**Figure 21.** ETS-NOCV – Deformation densities of orbitals for compound **Pre-2**. Red is electron loss (oxidation) and blue is electron gain (reduction).

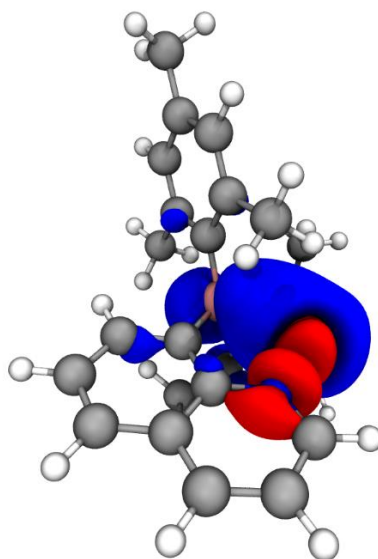


**Figure 22.** ETS-NOCV – Deformation densities of orbitals for **1**. Red is electron loss (oxidation) and blue is electron gain (reduction).

## CHAPTER FOUR

### Conclusions

Our computational investigation revealed a thermodynamically possible mechanism for the formation of an active catalyst, compound **1**, and the subsequent catalytic cycle under the given experimental conditions. The results are consistent with experimental observations. ETS-NOCV showed the proposed active catalyst (compound **1**) is an LMZ ligand which is stabilized by the shift of electron density from the electron-rich Pd to the electron-deficient B. Surprisingly, **Pre-2** gets destabilized by an electron density shift in the opposite direction. The next step would be to synthesize these compounds experimentally and create the novel complex sought after throughout this research.



## BIBLIOGRAPHY

- Harman, W. H.; Peters, J. C., Reversible H<sub>2</sub> Addition across a Nickel–Borane Unit as a Promising Strategy for Catalysis. *Journal of the American Chemical Society* **2012**, *134* (11), 5080-5082.
- Labinger, J. A., Tutorial on Oxidative Addition. *Organometallics* **2015**, *34* (20), 4784-4795.
- Frisch, M. J.; Trucks, G. W.; Schlegel, H. B.; Scuseria, G. E.; Robb, M. A.; Cheeseman, J. R.; Scalmani, G.; Barone, V.; Petersson, G. A.; Nakatsuji, H.; Li, X.; Caricato, M.; Marenich, A. V.; Bloino, J.; Janesko, B. G.; Gomperts, R.; Mennucci, B.; Hratchian, H. P.; Ortiz, J. V.; Izmaylov, A. F.; Sonnenberg, J. L.; Williams; Ding, F.; Lipparini, F.; Egidi, F.; Goings, J.; Peng, B.; Petrone, A.; Henderson, T.; Ranasinghe, D.; Zakrzewski, V. G.; Gao, J.; Rega, N.; Zheng, G.; Liang, W.; Hada, M.; Ehara, M.; Toyota, K.; Fukuda, R.; Hasegawa, J.; Ishida, M.; Nakajima, T.; Honda, Y.; Kitao, O.; Nakai, H.; Vreven, T.; Throssell, K.; Montgomery Jr., J. A.; Peralta, J. E.; Ogliaro, F.; Bearpark, M. J.; Heyd, J. J.; Brothers, E. N.; Kudin, K. N.; Staroverov, V. N.; Keith, T. A.; Kobayashi, R.; Normand, J.; Raghavachari, K.; Rendell, A. P.; Burant, J. C.; Iyengar, S. S.; Tomasi, J.; Cossi, M.; Millam, J. M.; Klene, M.; Adamo, C.; Cammi, R.; Ochterski, J. W.; Martin, R. L.; Morokuma, K.; Farkas, O.; Foresman, J. B.; Fox, D. J. *Gaussian 16 Rev. C.01*, Wallingford, CT, 2016.
- Weigend, F., Accurate Coulomb-fitting basis sets for H to Rn. *Physical Chemistry Chemical Physics* **2006**, *8* (9), 1057-1065.
- Weigend, F.; Ahlrichs, R., Balanced basis sets of split valence, triple zeta valence and quadruple zeta valence quality for H to Rn: Design and assessment of accuracy. *Physical Chemistry Chemical Physics* **2005**, *7* (18), 3297-3305.
- Zhao, Y.; Truhlar, D. G., A new local density functional for main-group thermochemistry, transition metal bonding, thermochemical kinetics, and noncovalent interactions. *The Journal of Chemical Physics* **2006**, *125* (19), 194101.
- Marenich, A. V.; Cramer, C. J.; Truhlar, D. G., Universal Solvation Model Based on Solute Electron Density and on a Continuum Model of the Solvent Defined by the Bulk Dielectric Constant and Atomic Surface Tensions. *The Journal of Physical Chemistry B* **2009**, *113* (18), 6378-6396.
- Lu, T.; Chen, F., Multiwfn: A multifunctional wavefunction analyzer. *Journal of Computational Chemistry* **2012**, *33* (5), 580-592.
- Mitoraj, M. P.; Michalak, A.; Ziegler, T., On the Nature of the Agostic Bond between Metal Centers and  $\beta$ -Hydrogen Atoms in Alkyl Complexes. An Analysis Based on the Extended

Transition State Method and the Natural Orbitals for Chemical Valence Scheme (ETS-NOCV). *Organometallics* **2009**, 28 (13), 3727-3733.

te Velde, G.; Bickelhaupt, F. M.; Baerends, E. J.; Fonseca Guerra, C.; van Gisbergen, S. J. A.; Snijders, J. G.; Ziegler, T., Chemistry with ADF. *Journal of Computational Chemistry* **2001**, 22 (9), 931-967.

Son, J.-H.; Pudenz, M. A.; Hoefelmeyer, J. D., Reactivity of the Bifunctional Ambiphilic Molecule 8-(dimesitylboryl)quinoline: Hydrolysis and Coordination to CuI, AgI and PdII. *Dalton Transactions* **2010**, 39 (45), 11081-11090.